

Sensitivity of Arctic CH₄ emissions to landscape wetness diminished by atmospheric feedbacks

Received: 29 July 2022

Accepted: 26 May 2023

Published online: 06 July 2023

 Check for updates

Philipp de Vrese¹✉, Lutz Beckebanze², Leonardo de Aro Galera^{3,4}, David Holl^{3,4}, Thomas Kleinen¹, Lars Kutzbach^{3,4}, Zoé Rehder¹ & Victor Brovkin^{1,4}

Simulations using land surface models suggest future increases in Arctic methane emissions to be limited by the thaw-induced drying of permafrost landscapes. Here we use the Max Planck Institute Earth System Model to show that this constraint may be weaker than previously thought owing to compensatory atmospheric feedbacks. In two sets of extreme scenario simulations, a modification of the permafrost hydrology resulted in diverging hydroclimatic trajectories that, however, led to comparable methane fluxes. While a wet Arctic showed almost twice the wetland area compared with an increasingly dry Arctic, the latter featured greater substrate availability due to higher temperatures resulting from reduced evaporation, diminished cloudiness and more surface solar radiation. Given the limitations of present-day models and the potential model dependence of the atmospheric response, our results provide merely a qualitative estimation of these effects, but they suggest that atmospheric feedbacks play an important role in shaping future Arctic methane emissions.

With the extent of perennially frozen ground already in decline as a result of climate change^{1–3}, more and more of the roughly 1,100–1,700 Gt of organic carbon stored in Arctic and sub-Arctic soils is being mobilized^{4–6}. At the same time, higher temperatures lead to a widespread change in vegetation known as Arctic greening⁷. The latter raises the uptake of atmospheric CO₂ by high-latitude plants, but also increases the amount of recently assimilated carbon available for microbial breakdown. While the strength of these feedbacks is uncertain, the warming of the terrestrial Arctic could turn the region from a carbon sink into a carbon source within the twenty-first century^{8–13}, notably reducing the remaining carbon budget for the more ambitious climate goals^{14–16}.

How much the Arctic—as a future net source of atmospheric carbon—may contribute to rising temperatures will depend on the fraction of carbon that is emitted as methane (CH₄) rather than CO₂. The global warming potential of CH₄ is an order of magnitude higher

than that of CO₂ (ref. 2), but the former is produced only during decomposition under anoxic conditions. Anaerobic decomposition requires water-saturated soils, making CH₄ emissions highly dependent on the soil hydrology in the Arctic and sub-Arctic zone^{17,18}. Permafrost plays a key role in the hydrological cycle of these regions because soil ice impedes the movement of water through the ground, often leading to the formation of a saturated zone above the permafrost table^{19–23}. At the same time, excess ice supports the formation of elevated landscape features with particularly dry conditions at the surface²⁴.

The latest generation of Earth system models (ESMs) represents some of the more general physical and biogeochemical permafrost-related processes and effects^{25–27}, and a number of land surface models (LSMs) are capable of simulating the present-day CH₄ fluxes from Arctic soils reasonably well²⁸. However, projections of future emissions are less well constrained^{13,18,29–37}, partly due to the

¹The Ocean in the Earth System, Max Planck Institute for Meteorology, Hamburg, Germany. ²Institute of Meteorology and Climate Research, Karlsruhe Institute of Technology, Karlsruhe, Germany. ³Institute of Soil Science, Universität Hamburg, Hamburg, Germany. ⁴Center for Earth System Research and Sustainability (CEN), Universität Hamburg, Hamburg, Germany. ✉e-mail: philipp.de-vrese@mpimet.mpg.de

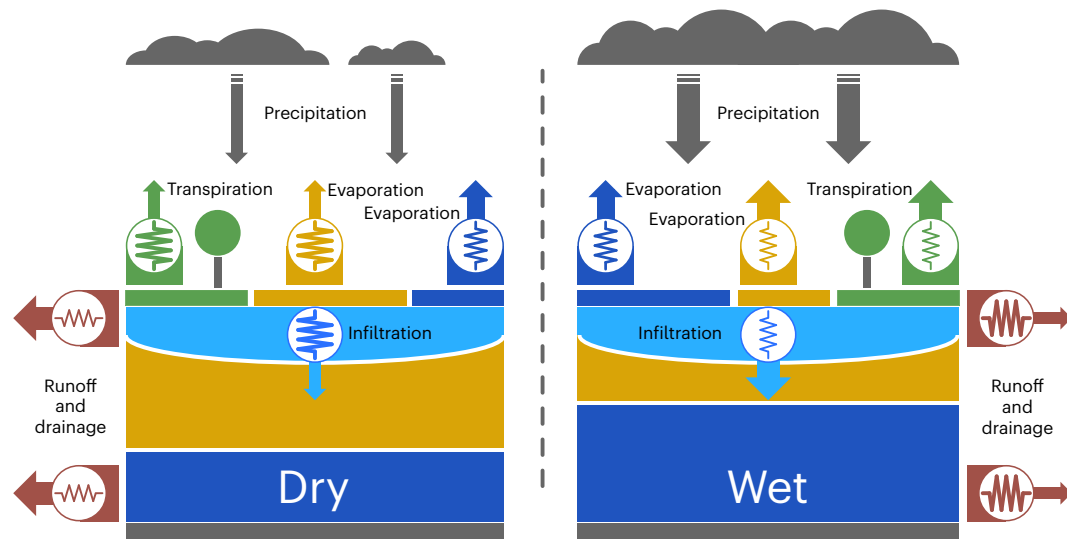


Fig. 1 | Dry and wet set-up. Qualitative comparison between the simulated hydrological cycle in the dry and wet JSBACH set-ups, following the degradation of the near-surface permafrost. Shown are the hydrological fluxes from the land surface and the soil, namely transpiration (green), bare-soil evaporation (yellow), evaporation from wetlands (dark blue), infiltration (light blue), and surface runoff and drainage (red). The size of the resistance symbols indicates whether the parameter settings in a set-up facilitate a certain process (indicated by a

small resistance symbol) or impede it (indicated by a large resistance symbol). At the same saturation of the soil (or, for infiltration and surface runoff, the same precipitation), a high resistance results in small fluxes (indicated by thin arrows), while a low resistance leads to a large flux (indicated by thick arrows). Finally, the size of the cloud and the thickness of the grey arrows indicate the atmospheric response to the evapotranspiration flux, while the size of the dark blue area in the belowground column indicates the amount of water stored in the soil.

large uncertainty in the hydroclimatic response to climate change. Most ESMs agree that the Arctic and sub-Arctic region will receive more precipitation in a warmer world³⁸, which would suggest wetter soils in the future. At the same time, higher near-surface temperatures result in larger evapotranspiration rates, while a warming-induced reduction in the extent and thickness of permafrost facilitates drainage and could lead to a desiccation of the thawing ground^{39,40}. With the net effect of these opposing processes being highly uncertain, present-generation LSMs do not even agree on whether high-latitude soils will contain more or less water in the future⁴¹.

It is generally assumed that wetter conditions in the Arctic and sub-Arctic zone would result in higher terrestrial CH₄ emissions as the extent of fully (water) saturated soils—hence the CH₄-producing areas—is larger. Using an LSM with prescribed atmospheric conditions, Lawrence et al.⁴² showed that the warming-induced twenty-first-century increase in high-latitude CH₄ emissions could be twice as large if the soils remain highly saturated after the permafrost is degraded. But, while the correlation between the wetland area and soil CH₄ production certainly constitutes an important driver, it is not the only way in which the permafrost hydrology affects the future CH₄ fluxes. The hydrological state of the soil also has a profound impact on the land–atmosphere interactions, which in turn control the near-surface climate in the high latitudes⁴³. Thus, with many aspects of the carbon cycle depending on the near-surface temperatures and precipitation rates, the permafrost-thaw-induced changes to the soil hydrology also affect future CH₄ emissions by altering the land–atmosphere feedbacks. The effects of changing land–atmosphere interactions on the Arctic CH₄ emissions, however, have never been investigated.

In the following, we address this research gap using an adapted version of the Max Planck Institute (MPI) for Meteorology ESM, more specifically of the MPI-ESM1.2 (refs. 13,43,44). With this version of the MPI-ESM we can simulate the terrestrial CH₄ fluxes that arise from varying degrees of ‘wetness’ of the northern permafrost regions, taking into account all the land–atmosphere feedbacks that these diverging hydrological conditions entail. For a high warming scenario (that is, Shared Socioeconomic Pathway 5 and Representative Concentration Pathway 8.5 (SSP5-8.5)^{45–47}), we compare the projected

twenty-first-century CH₄ emissions of two sets of simulations based on simplified extreme set-ups. These simulations enclose the plausible parameter space between ‘wet’ and increasingly ‘dry’ conditions as represented in the Jena Scheme for Biosphere Atmosphere Coupling in Hamburg (JSBACH), the land component of the MPI-ESM. The wet simulations assume favourable infiltration properties in the permafrost region combined with a high drainage resistance, resulting in wetter soils, and a low resistance with respect to evapotranspiration, which leads to an intense local moisture recycling. In contrast, the configuration of the dry simulations leads to a weaker local moisture recycling, in combination with low infiltration rates and low drainage resistance, resulting in increasingly dry soils whenever the near-surface permafrost is degraded (Fig. 1 and Supplementary Tables 1 and 2). A more detailed overview over the experimental set-up is given in Methods, while the ‘Results’ and ‘Discussion and conclusions’ present our results and discuss the pathways by which the soil hydrology in permafrost regions affects the CH₄ emissions inside and outside of the terrestrial Arctic. It should be noted that, in the following, we mainly discuss the differences between the two hydroclimatic trajectories and describe the resulting effects on CH₄ emission in relative terms; for example, when we refer to a ‘cooling’, this should be understood as temperatures being lower in one simulation than in another simulation but not necessarily as an absolute temperature reduction.

Results

The twenty-first-century warming that results from the high emissions scenario SSP5-8.5 will lead to a substantial decline in the extent and thickness of the near-surface permafrost in the Arctic and sub-Arctic zone. The hydroclimatic response to this permafrost degradation depends on the ability of the soils to retain water after the effectively impermeable, perennial ground ice disappears and on the resulting land–atmosphere interactions (Supplementary Fig. 1). In the wet scenario, the northern permafrost regions show a more intense hydrological cycle, with the high drainage resistance and infiltration rates maintaining comparatively wet soils. Higher evapotranspiration rates cool the surface and the boundary layer, while increasing the moisture transport into the atmosphere. Lower temperatures, in combination

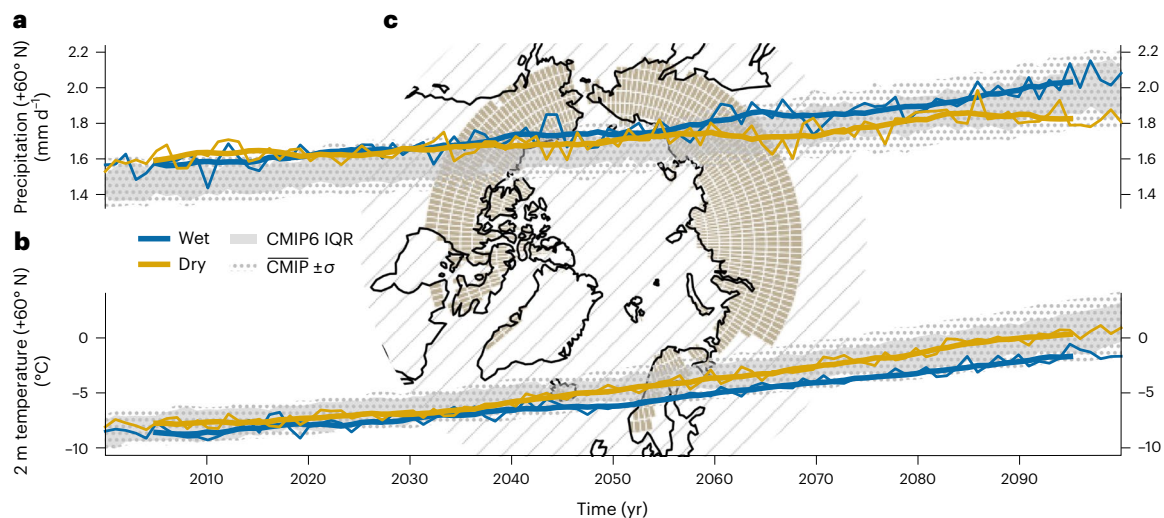


Fig. 2 | Effects of soil hydrological conditions on the simulated state of the atmosphere in permafrost regions. **a**, Simulated twenty-first-century precipitation rates for the wet (blue line) and the dry (yellow line) set-up. Shown are the average rates over the Arctic permafrost region (shown in brown in **c**). The thin lines show annual averages, while the thick lines show the 10 year

running mean. The shaded area indicates the interquartile range (IQR) of the CMIP6 model ensemble and the dotted area indicates the range of the ensemble mean $\pm 1\sigma$; these are two commonly used measures for the ensemble spread⁴³. **b**, The same as in **a**, but for the 2 m temperature. **c**, Permafrost-affected regions north of 60° N.

with a higher atmospheric water content, raise the relative humidity, resulting in more extensive cloud cover and more precipitation than in the dry scenario (Fig. 2a). The additional precipitation, in turn, leads to a larger extent of inundated areas and increases the available soil moisture, closing the positive evaporation–precipitation feedback loop. At the same time, the more extensive cloud cover reduces the incoming solar radiation, which diminishes the available energy at the surface. This limits the latent heat flux, including evaporation from wetlands, and hence contributes to the larger spatial extent of water-logged soils. In addition, the reduction in available energy lowers the sensible heat flux, further raising the atmospheric relative humidity, and substantially reduces the twenty-first-century warming trend (Fig. 2b). It should be noted that our set-ups strongly reduce the complexity of the high-latitude land–atmosphere interactions, with the resulting impact on climate being, to a certain degree, model dependent. However, both the wet and dry simulations remain within the uncertainty range of the Coupled Model Intercomparison Project Phase 6 (CMIP6) ensemble and we consider the two trajectories to be equally plausible climate futures of our planet.

When accounting for the abovementioned climate feedbacks, we find a spatially non-uniform effect of the soil hydrological conditions on the twenty-first-century trend in terrestrial CH₄ emissions. Compared with the dry scenario, the wet scenario shows larger end-of-the-century CH₄ fluxes from the organic-rich soils in the West Siberian Plain, but there is no clear signal in the North American Arctic and the emissions are actually smaller in northern Europe and in the Lena catchment (Fig. 3a). Aggregated across the northern permafrost regions, the average increase in the CH₄ fluxes is extremely similar for the two trajectories (Fig. 3b) and, for a climate stabilization under end-of-the-century greenhouse gas concentrations, our model even produces slightly larger emissions if the soils show a pronounced drying trend in response to the permafrost degradation (see below). This suggests that the general hypothesis of wetter conditions necessarily leading to higher future CH₄ emissions may not be valid, despite the extent of the CH₄-producing areas remaining comparatively constant in the wet scenario and decreasing substantially in the dry simulations (Fig. 3c,d). While these results appear counterintuitive, they can be explained by the differences in the near-surface climate resulting from the diverging hydrological responses to permafrost degradation.

The aerobic and anaerobic respiration rates depend on the climate conditions directly, because of the temperature and moisture dependence of the soil microbial activity, and indirectly, because the prevailing temperatures and precipitation rates affect substrate availability (see below). In particular, warming during the twenty-first century leads to an increase in soil respiration rates, and this increase is substantially larger for the warmer dry trajectory (Fig. 4a). In fact, the higher temperatures in this scenario raise the respiration rates to such a degree that the effect of shrinking wetlands on the anaerobic respiration is offset by a combination of higher decomposition rates and increased substrate availability in the remaining saturated soils. Consequently, the fraction of soil organic matter that decomposes under anoxic conditions is increasingly lower in the dry than in the wet trajectory, but the total amount of CH₄ produced in high-latitude soils is comparable between the two (Fig. 4b). In other words, the main reason why future CH₄ emissions may not necessarily be higher if the conditions stay comparatively wet—and the fraction of saturated soils remains large—is that the additional evapotranspiration and ensuing climate feedbacks cool the continental Arctic, slowing down microbial decomposition processes and reducing the overall substrate availability.

Another important factor is the differences in vegetation dynamics. These dynamics are mainly driven by the temperature differences between the two scenarios and lead to a higher root density and more extensive graminoid cover in the dry scenario (Supplementary Fig. 4). There are two major pathways by which CH₄ is transported from the deeper anoxic soil layers towards the surface, with the ratio of CH₄ emitted and CH₄ produced being highly dependent on the transport process. One of these mechanisms is the diffusive transport through the soil pore spaces. However, even in saturated soils, most of the CH₄ that diffuses upwards is oxidized by aerobic methanotrophic bacteria in near-surface layers. Thus, the largest CH₄ fluxes at the soil–atmosphere interface do not result from vertical diffusion, but from plant-mediated transport, the second major transport mechanism. Here CH₄ diffuses from the CH₄-enriched soil pore space into the roots and is transported through the aerenchyma to the atmosphere. Herbaceous plants are particularly effective at this, and a higher graminoid fraction increases plant-mediated transport. In combination, the higher root density and graminoid fraction in the dry simulations lead to CH₄ fluxes similar to those in the wet simulations, despite lower CH₄ production rates.

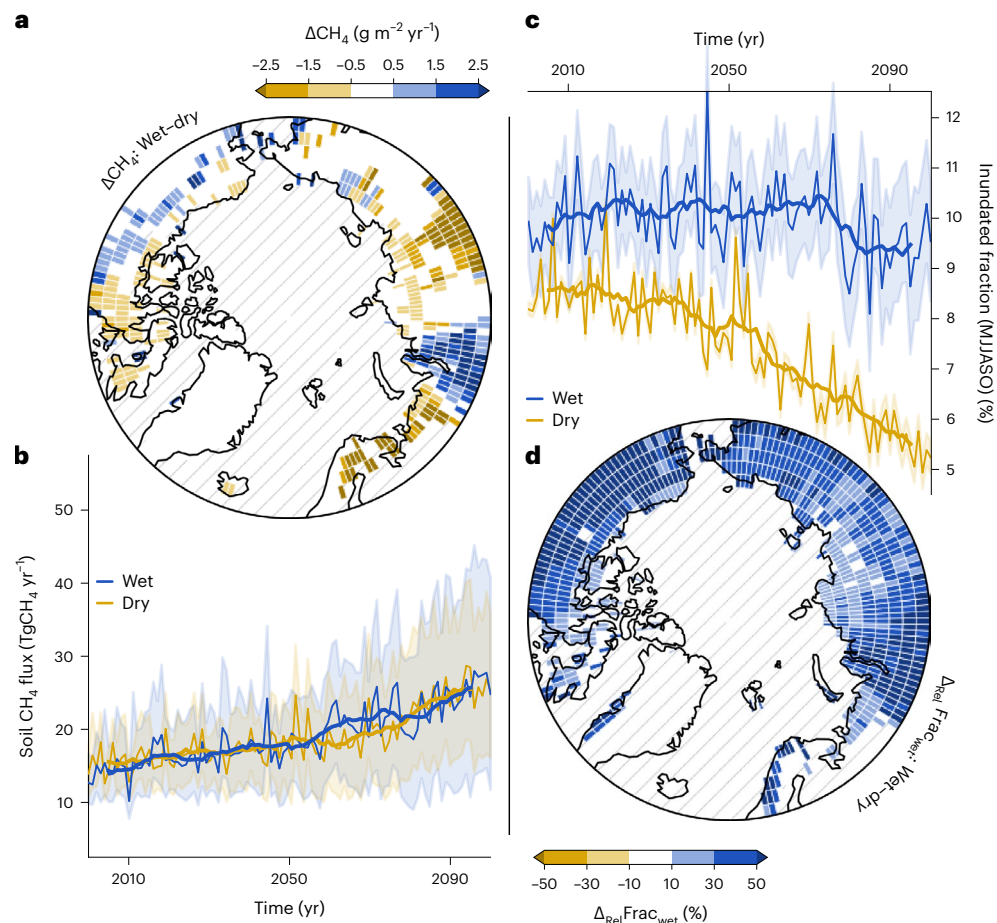


Fig. 3 | Simulated trends in Arctic CH₄ emissions and wetland area.

a, Difference in the soil CH₄ emissions between the wet and dry scenarios averaged over the period 2080–2100. **b**, Simulated soil CH₄ emissions averaged over the Arctic permafrost regions (Fig. 2c) for the wet and dry scenarios. The blue lines show the mean of the ensemble of wet JSBACH simulations, with the thick line indicating the 10 year running mean. The shaded area shows the

spread between the ensemble minimum and maximum. The dry ensemble is shown in yellow. **c**, The same as in **b**, but for the simulated extent of waterlogged soils during the season May to October (MJJASO); that is, those areas where soil organic matter decomposes under anoxic conditions. **d**, The same as in **a**, but for the relative difference in the extent of waterlogged soils ($\Delta_{\text{RelFrac}}^{\text{Wet-dry}}$).

This leaves the question of what is sustaining the increased substrate availability in the dry trajectory. The increased incoming solar radiation raises the temperatures in the soil, which exposes more of the formerly frozen soil organic matter to conditions under which it can be decomposed (Fig. 4c). More importantly, the higher near-surface temperatures also prolong the growing season (Fig. 4d). Here the increase in growing degree days in the dry scenario is so pronounced that it predominates over the effects due to increased water stress resulting from the permafrost-thaw-induced drying of the soil (Fig. 4e). As a result, the net primary productivity in the dry simulations almost triples during the twenty-first century, while the respective effect in the colder wet scenario is substantially weaker (Fig. 4f). Thus, we find that it is the warmer climate resulting from the drier conditions that leads to a greener (more productive) Arctic, rather than higher (plant) water availability under wetter conditions, as previously assumed⁴⁸. The higher productivity and larger carbon inputs into the soil in the dry scenario offset the higher respiration rates, which leads to a similar net ecosystem exchange in the two scenarios (Fig. 4g), indicating that the similar CH₄ emissions in the two trajectories are not merely a transient phenomenon resulting from a deeper active layer in the warmer dry simulations (Supplementary Fig. 5). To confirm this, we extended the simulations for another 100 years, stabilizing the climate conditions at the end of the twenty-first century. Under these non-transient atmospheric conditions, the net ecosystem exchange in the two trajectories

converges to a similar equilibrium (Fig. 4h), while the soil CH₄ emissions in the dry simulations are even slightly higher than the ones in the wet simulations (Fig. 4i).

The above results should be regarded as a qualitative approximation of the future CH₄ emissions rather than an attempt at an exact quantification. The latter cannot be obtained with the present experimental set-up due to the limitations that JSBACH shares with other coarse-resolution LSMs. Nonetheless, when using observation-based temperature–emission relationships (Fig. 5a) to estimate the future wetland CH₄ fluxes for the two climate trajectories, these agree well with our findings. For the near-surface temperatures that result from a climate stabilization under end-of-the-century greenhouse gas concentrations, the estimated CH₄ emissions from a given wetland area are roughly twice as large for the warmer dry scenario (Fig. 5b). Thus, even if half the Arctic wetlands were to disappear, the respective CH₄ fluxes could be similar to those of a wet scenario with a stable wetland extent but lower temperatures. Furthermore, while JSBACH accounts for the effects of inundated areas on the state of the soil and the land–atmosphere interactions, it does not explicitly represent the thermodynamics and biochemistry of (shallow) water bodies. Instead, we used the recently developed Methane Emissions from Ponds (MeEP) model⁴⁹ to estimate the emissions from polygonal tundra ponds with a high pond density. As soils below bodies of water are always waterlogged, the CH₄ emissions for a given pond area are largely determined by

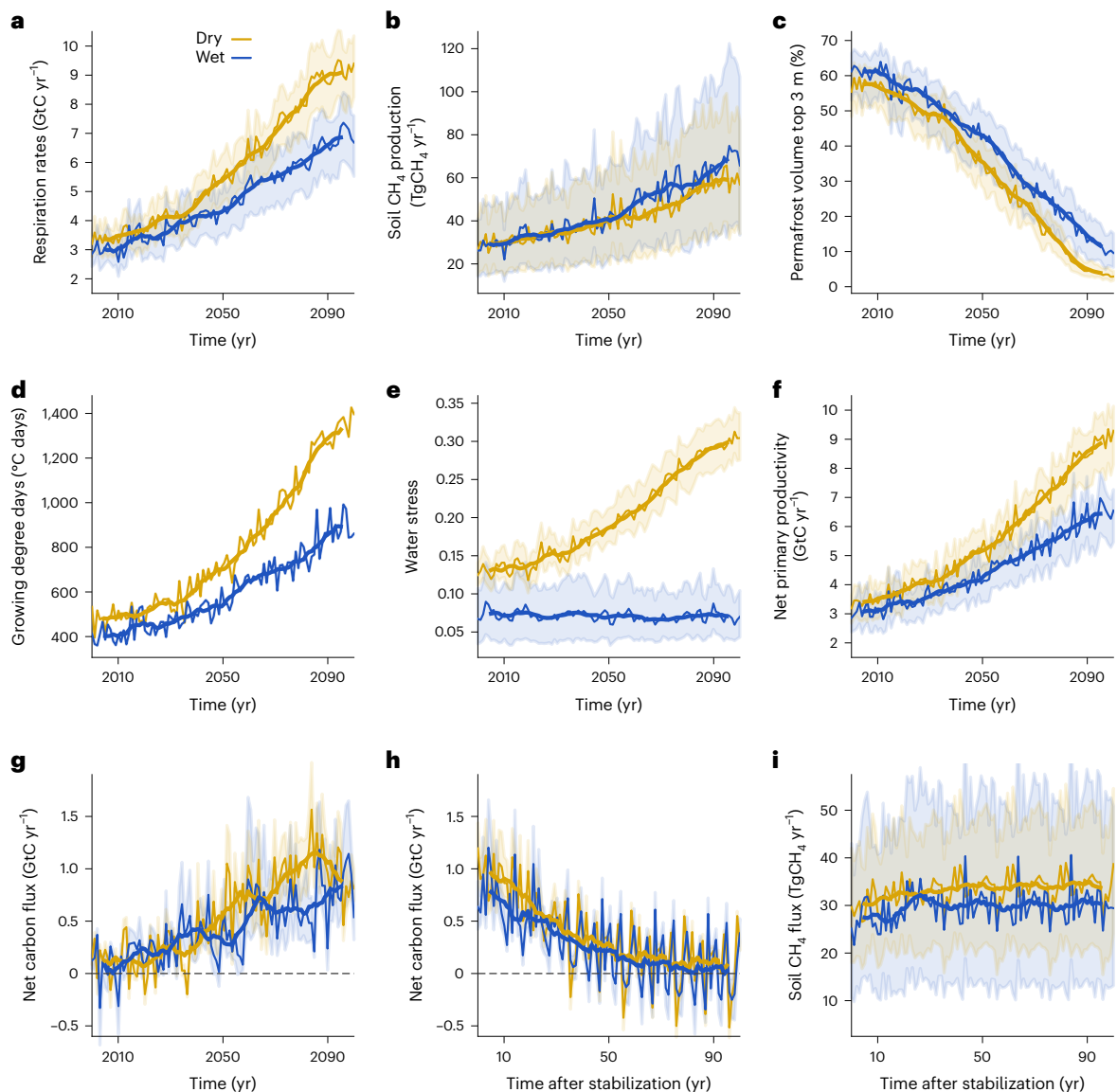


Fig. 4 | Drivers of future CH₄ fluxes in the northern permafrost regions.

a, b, c, d, e, f, g. Simulated (aerobic and anaerobic) soil respiration rates in the northern permafrost region. The blue lines show the mean of the ensemble of wet JSBACH simulations, with the thick line indicating the 10 year running mean. The shaded area shows the spread between the ensemble minimum and maximum. The dry ensemble is shown in yellow. **b–g.** The same as in **a**, but for the CH₄ produced in

the soil (**b**), near-surface permafrost volume (**c**), growing degree days (**d**), water stress (**e**), net primary productivity (**f**) and net ecosystem exchange (positive into the atmosphere) (**g**). **h, i.** The net ecosystem exchange (**h**) and soil CH₄ emissions (**i**) are shown for a 100 year period under non-transient atmospheric conditions, corresponding to a climate stabilization under the greenhouse gas concentrations at the end of the twenty-first century.

the amount of organic matter available for decomposition, with the model projecting a higher plant productivity and substrate availability in the dry scenario than in the wet scenario. Thus, the emissions from a given surface area are substantially higher in the dry scenario (with slightly different ratios for overgrown and open water surfaces; Fig. 5c), indicating that, even for a pronounced loss in their spatial extent, the emissions from polygonal tundra ponds may be similar to those under wet future conditions.

Discussion and conclusions

Our findings indicate that the magnitude of future Arctic CH₄ emissions may be less dependent on the hydrological state of the soils than previously thought, which can be interpreted in a positive or a negative way: a positive conclusion is that our results support the view that the warming-induced thawing of the Arctic permafrost will most likely not result in a vast increase in terrestrial CH₄ emissions^{12,37}.

Our simulations rather indicate that, even if the high latitudes maintain wet conditions in a high warming scenario, the associated cooling effects could limit the increase in the terrestrial CH₄ emissions. A negative interpretation of our results would, however, be that even a pronounced permafrost-thaw-induced drying of the landscape and the resulting decline in the spatial wetland extent may not prevent terrestrial CH₄ emissions from rising in a warmer future. Thus, while a drastic rise in CH₄ emissions seems unlikely, a pronounced increase appears inevitable: either wet and cold conditions lead to a comparatively inert carbon cycle characterized by long turnover times, in which, however, a large fraction of the emitted carbon is being released from the soils as CH₄, or drier and warmer future conditions result in a more active carbon cycle and short turnover times, but with only a small fraction of the soil carbon being emitted as CH₄.

While we find that the CH₄ fluxes in the high latitudes may be similar for a wet and a dry future Arctic, this is not necessarily the case for

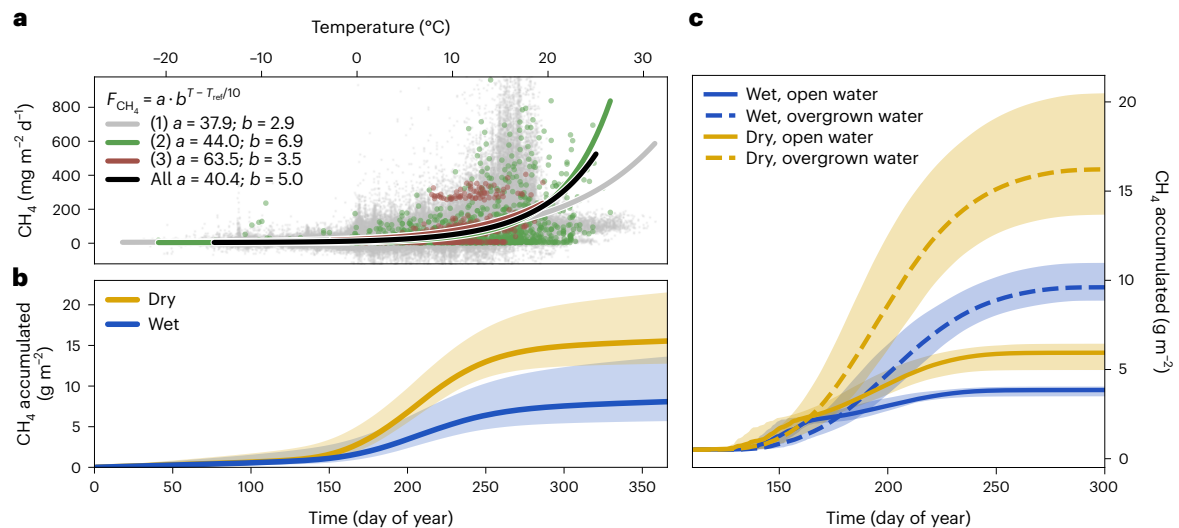


Fig. 5 | Observation-based estimates. **a**, Observed temperature dependence of CH_4 emissions for wetland sites north of 45° N based on (1) ref. 56 (grey), (2) ref. 57 (green), (3) ref. 58 (brown) and a combination of (1) to (3) (black). Dots represent the measured values of emissions and temperatures while the lines show the fitted relationships. **b**, Projected CH_4 emissions for a climate stabilization after 2100 based on simulated soil temperatures and the fitted, observation-based temperature dependence (from **a**). Shown are the accumulated CH_4 emissions for the 30 year mean annual temperature cycle averaged over the Arctic permafrost region. The solid lines indicate CH_4 emissions for the CH_4 temperature

dependence based on all datasets combined, while the spread is based on the minimum and maximum CH_4 values derived for the temperature dependencies from (1) to (3). **c**, Simulated pond CH_4 emissions, for example, polygonal tundra sites in the Lena River Delta (Siberia, Russia), on Bylot Island (Nunavut, Canada) and Barrow Peninsula (Alaska, USA), with the shaded area showing the range between the minimum and maximum emissions at the sites and lines showing the respective mean. The simulations use the newly developed MeEP model⁴⁹ and the simulated temperatures of the wet and dry scenarios for a climate stabilization under greenhouse gas concentrations corresponding to 2100 (SSP5-8.5).

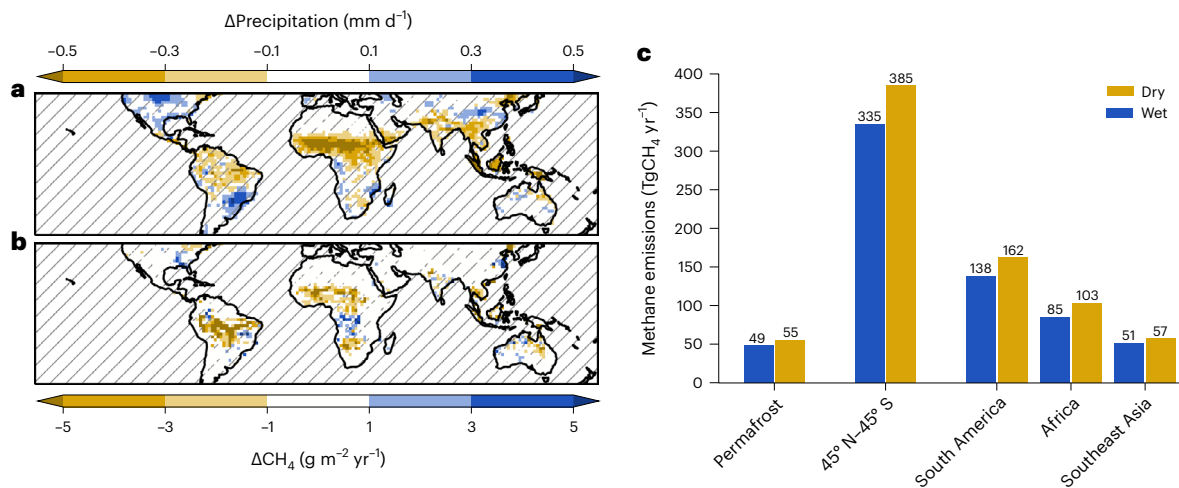


Fig. 6 | Global CH_4 emissions. **a**, Difference in annual mean precipitation between the wet and dry trajectories for a climate stabilization under greenhouse gas concentrations corresponding to 2100 (SSP5-8.5). The diagonal lines cover areas of non-significant differences ($P > 0.05$) and oceans. **b**, The same as in **a**, but

for annual mean CH_4 emissions. **c**, CH_4 budgets for permafrost regions north of 45° N, the latitudes between 45° N and 45° S, South America, Africa and Southeast Asia. Note that the emissions in non-permafrost regions were estimated using a different model version, the detailed description of which is given in ref. 59.

the natural CH_4 emission outside of the northern permafrost regions. The global (wetland) CH_4 budget is dominated by the CH_4 fluxes from tropical wetlands, which our simulations show to be affected by the land-atmosphere interactions in the northern permafrost regions. This is mainly because the rate of warming of the Arctic relative to that at the Equator determines the latitudinal temperature gradient. This gradient, in turn, affects a number of important features of the global climate system, most notably, the location and oscillation of the intertropical convergence zone and the West African monsoon. Here a drier, warmer Arctic could lead to a weaker temperature gradient and more precipitation in the tropics (Fig. 6a). Increased tropical

precipitation leads to a larger wetland extent, with our findings suggesting that the resulting impact on tropical CH_4 emissions could be several times larger than the effect on the CH_4 fluxes in the Arctic and sub-Arctic zone (Fig. 6b,c). Thus, the hydroclimatic trajectory of the permafrost region indeed appears to play an important role in shaping future CH_4 emissions, but the most important effects may manifest outside of the high latitudes.

Finally, we acknowledge that JSBACH, as with most LSMs, has a number of important limitations. Our model captures the fundamental physical and biophysical processes in the high latitudes, but does not account for the small-scale hydrological and geomorphological

mechanisms, such as thermokarst features, that play a key role in the dynamics of permafrost-affected landscapes and often determine the interactions between biogeophysical and biogeochemical factors. Most importantly, the model captures the carbon release resulting from gradual changes in seasonally thawed soils, but neglects nonlinear and abrupt change processes that are often spatially and temporally very confined but hold the potential to modulate the carbon emissions of entire regions^{34,50–54}. Furthermore, while peatlands make up the largest part of the high-latitude wetlands⁵⁵, JSBACH does not represent processes specific to bogs and fens and, most importantly, cannot capture the particularly large drainage resistance of these wetland types. Given their high relevance for soil CH₄ emissions, the lack of representation of the above processes in our model has most certainly had an effect on our results.

Online content

Any methods, additional references, Nature Portfolio reporting summaries, source data, extended data, supplementary information, acknowledgements, peer review information; details of author contributions and competing interests; and statements of data and code availability are available at <https://doi.org/10.1038/s41558-023-01715-3>.

References

- Brown, J. & Romanovsky, V. E. Report from the International Permafrost Association: state of permafrost in the first decade of the 21st century. *Permafr. Periglac. Process.* **19**, 255–260 (2008).
- Stocker, T. et al. in *Climate Change 2013: The Physical Science Basis* (eds Stocker, T. et al.) 33–115 (Cambridge Univ. Press, 2013).
- Biskaborn, B. K. et al. Permafrost is warming at a global scale. *Nat. Commun.* **10**, 264 (2019).
- Zimov, S. A. et al. Permafrost carbon: stock and decomposability of a globally significant carbon pool. *Geophys. Res. Lett.* <https://doi.org/10.1029/2006gl027484> (2006).
- Tarnocai, C. et al. Soil organic carbon pools in the northern circumpolar permafrost region. *Global Biogeochem. Cy.* <https://doi.org/10.1029/2008gb003327> (2009).
- Hugelius, G. et al. Estimated stocks of circumpolar permafrost carbon with quantified uncertainty ranges and identified data gaps. *Biogeosciences* **11**, 6573–6593 (2014).
- Myers-Smith, I. H. et al. Complexity revealed in the greening of the arctic. *Nat. Clim. Change* **10**, 106–117 (2020).
- Schaefer, K., Lantuit, H., Romanovsky, V. E., Schuur, E. A. G. & Witt, R. The impact of the permafrost carbon feedback on global climate. *Environ. Res. Lett.* **9**, 085003 (2014).
- McGuire, A. D. et al. Dependence of the evolution of carbon dynamics in the northern permafrost region on the trajectory of climate change. *Proc. Natl Acad. Sci. USA* **115**, 3882–3887 (2018).
- Lenton, T. M. et al. Climate tipping points—too risky to bet against. *Nature* **575**, 592–595 (2019).
- Turetsky, M. R. et al. Permafrost collapse is accelerating carbon release. *Nature* **569**, 32–34 (2019).
- Bruhwyler, L., Parmentier, F.-J. W., Crill, P., Leonard, M. & Palmer, P. I. The Arctic carbon cycle and its response to changing climate. *Curr. Clim. Change Rep.* **7**, 14–34 (2021).
- de Vrese, P., Stacke, T., Kleinen, T. & Brovkin, V. Diverging responses of high-latitude CO₂ and CH₄ emissions in idealized climate change scenarios. *Cryosphere* **15**, 1097–1130 (2021).
- Comyn-Platt, E. et al. Carbon budgets for 1.5 and 2 °C targets lowered by natural wetland and permafrost feedbacks. *Nat. Geosci.* **11**, 568–573 (2018).
- Gasser, T. et al. Path-dependent reductions in CO₂ emission budgets caused by permafrost carbon release. *Nat. Geosci.* **11**, 830–835 (2018).
- Natali, S. M. et al. Permafrost carbon feedbacks threaten global climate goals. *Proc. Natl Acad. Sci. USA* **118**, e2100163118 (2021).
- Olefeldt, D., Turetsky, M. R., Crill, P. M. & McGuire, A. D. Environmental and physical controls on northern terrestrial methane emissions across permafrost zones. *Glob. Change Biol.* **19**, 589–603 (2012).
- Knoblauch, C., Beer, C., Liebner, S., Grigoriev, M. N. & Pfeiffer, E.-M. Methane production as key to the greenhouse gas budget of thawing permafrost. *Nat. Clim. Change* **8**, 309–312 (2018).
- Woo, M.-K., Kane, D. L., Carey, S. K. & Yang, D. Progress in permafrost hydrology in the new millennium. *Permafr. Periglac. Process.* **19**, 237–254 (2008).
- Painter, S. L., Moulton, J. D. & Wilson, C. J. Modeling challenges for predicting hydrologic response to degrading permafrost. *Hydrogeol. J.* **21**, 221–224 (2012).
- Swenson, S. C., Lawrence, D. M. & Lee, H. Improved simulation of the terrestrial hydrological cycle in permafrost regions by the community land model. *J. Adv. Model. Earth Syst.* <https://doi.org/10.1029/2012ms000165> (2012).
- Toride, N., Watanabe, K. & Hayashi, M. Special section: progress in modeling and characterization of frozen soil processes. *Vadose Zone J.* **12**, 1–4 (2013).
- Walvoord, M. A. & Kurylyk, B. L. Hydrologic impacts of thawing permafrost—a review. *Vadose Zone J.* **15**, 1–20 (2016).
- Karjalainen, O. et al. High potential for loss of permafrost landforms in a changing climate. *Environ. Res. Lett.* **15**, 104065 (2020).
- McGuire, A. D. et al. Variability in the sensitivity among model simulations of permafrost and carbon dynamics in the permafrost region between 1960 and 2009. *Global Biogeochem. Cy.* **30**, 1015–1037 (2016).
- Chadburn, S. E. et al. Carbon stocks and fluxes in the high latitudes: using site-level data to evaluate Earth system models. *Biogeosciences* **14**, 5143–5169 (2017).
- Blyth, E. M. et al. Advances in land surface modelling. *Curr. Clim. Change Rep.* **7**, 45–71 (2021).
- Saunois, M. et al. The global methane budget 2000–2017. *Earth Syst. Sci. Data* **12**, 1561–1623 (2020).
- Burke, E. J., Hartley, I. P. & Jones, C. D. Uncertainties in the global temperature change caused by carbon release from permafrost thawing. *Cryosphere* **6**, 1063–1076 (2012).
- von Deimling, T. S. et al. Estimating the near-surface permafrost-carbon feedback on global warming. *Biogeosciences* **9**, 649–665 (2012).
- Gao, X. et al. Permafrost degradation and methane: low risk of biogeochemical climate-warming feedback. *Environ. Res. Lett.* **8**, 035014 (2013).
- Koven, C. D., Lawrence, D. M. & Riley, W. J. Permafrost carbon-climate feedback is sensitive to deep soil carbon decomposability but not deep soil nitrogen dynamics. *Proc. Natl Acad. Sci. USA* **112**, 3752–3757 (2015).
- Koven, C. D. et al. A simplified, data-constrained approach to estimate the permafrost carbon-climate feedback. *Phil. Trans. R. Soc. A* **373**, 20140423 (2015).
- Anthony, K. W. et al. 21st-century modeled permafrost carbon emissions accelerated by abrupt thaw beneath lakes. *Nat. Commun.* **9**, 3262 (2018).
- Oh, Y. et al. Reduced net methane emissions due to microbial methane oxidation in a warmer Arctic. *Nat. Clim. Change* **10**, 317–321 (2020).
- Yokohata, T. et al. Future projection of greenhouse gas emissions due to permafrost degradation using a simple numerical scheme with a global land surface model. *Prog. Earth Planet. Sci.* **7**, 56 (2020).
- Anisimov, O. & Zimov, S. Thawing permafrost and methane emission in Siberia: synthesis of observations, reanalysis, and predictive modeling. *Ambio* **50**, 2050–2059 (2021).

38. Tebaldi, C. et al. Climate model projections from the Scenario Model Intercomparison Project (ScenarioMIP) of CMIP6. *Earth Syst. Dyn.* **12**, 253–293 (2021).
39. Bring, A. et al. Arctic terrestrial hydrology: a synthesis of processes, regional effects, and research challenges. *J. Geophys. Res. Biogeosci.* **121**, 621–649 (2016).
40. Kreplin, H. N. et al. Arctic wetland system dynamics under climate warming. *WIREs Water* **8**, e1526 (2021).
41. Andresen, C. G. et al. Soil moisture and hydrology projections of the permafrost region – a model intercomparison. *Cryosphere* **14**, 445–459 (2020).
42. Lawrence, D. M., Koven, C. D., Swenson, S. C., Riley, W. J. & Slater, A. G. Permafrost thaw and resulting soil moisture changes regulate projected high-latitude CO₂ and CH₄ emissions. *Environ. Res. Lett.* **10**, 094011 (2015).
43. de Vrese, P. et al. Representation of soil hydrology in permafrost regions may explain large part of inter-model spread in simulated Arctic and subarctic climate. *Cryosphere* **17**, 2095–2118 (2023).
44. Mauritsen, T. et al. Developments in the MPI-M Earth System Model version 1.2 (MPI-ESM1.2) and its response to increasing CO₂. *J. Adv. Model. Earth Syst.* **11**, 998–1038 (2019).
45. van Vuuren, D. P. et al. The representative concentration pathways: an overview. *Climatic Change* **109**, 5–31 (2011).
46. Riahi, K. et al. The shared socioeconomic pathways and their energy, land use, and greenhouse gas emissions implications: an overview. *Glob. Environ. Change* **42**, 153–168 (2017).
47. Hausfather, Z. & Peters, G. P. Emissions—the ‘business as usual’ story is misleading. *Nature* **577**, 618–620 (2020).
48. Miner, K. R. et al. Permafrost carbon emissions in a changing Arctic. *Nat. Rev. Earth Environ.* **3**, 55–67 (2022).
49. Rehder, Z. *Measuring and Modeling of Methane Emissions from Ponds in High Latitudes*. PhD thesis, Univ. Hamburg (2022).
50. Serreze, M. C. et al. Observational evidence of recent change in the northern high-latitude environment. *Climatic Change* **46**, 159–207 (2000).
51. Jorgenson, M. T., Shur, Y. L. & Pullman, E. R. Abrupt increase in permafrost degradation in Arctic Alaska. *Geophys. Res. Lett.* <https://doi.org/10.1029/2005gl024960> (2006).
52. O’Donnell, J. A. et al. The effects of permafrost thaw on soil hydrologic, thermal, and carbon dynamics in an Alaskan peatland. *Ecosystems* **15**, 213–229 (2011).
53. Liljedahl, A. K. et al. Pan-Arctic ice-wedge degradation in warming permafrost and its influence on tundra hydrology. *Nat. Geosci.* **9**, 312–318 (2016).
54. Turetsky, M. R. et al. Carbon release through abrupt permafrost thaw. *Nat. Geosci.* **13**, 138–143 (2020).
55. Olefeldt, D. et al. The Boreal–Arctic Wetland and Lake Dataset (BAWLD). *Earth Syst. Sci. Data* **13**, 5127–5149 (2021).
56. Delwiche, K. B. et al. FLUXNET-CH₄: a global, multi-ecosystem dataset and analysis of methane seasonality from freshwater wetlands. *Earth Syst. Sci. Data* **13**, 3607–3689 (2021).
57. Chen, H., Xu, X., Fang, C., Li, B. & Nie, M. Differences in the temperature dependence of wetland CO₂ and CH₄ emissions vary with water table depth. *Nat. Clim. Change* **11**, 766–771 (2021).
58. Yvon-Durocher, G. et al. Methane fluxes show consistent temperature dependence across microbial to ecosystem scales. *Nature* **507**, 488–491 (2014).
59. Kleinen, T., Mikolajewicz, U. & Brovkin, V. Terrestrial methane emissions from the last glacial maximum to the preindustrial period. *Climate* **16**, 575–595 (2020).

Publisher’s note Springer Nature remains neutral with regard to jurisdictional claims in published maps and institutional affiliations.

Open Access This article is licensed under a Creative Commons Attribution 4.0 International License, which permits use, sharing, adaptation, distribution and reproduction in any medium or format, as long as you give appropriate credit to the original author(s) and the source, provide a link to the Creative Commons license, and indicate if changes were made. The images or other third party material in this article are included in the article’s Creative Commons license, unless indicated otherwise in a credit line to the material. If material is not included in the article’s Creative Commons license and your intended use is not permitted by statutory regulation or exceeds the permitted use, you will need to obtain permission directly from the copyright holder. To view a copy of this license, visit <http://creativecommons.org/licenses/by/4.0/>.

© The Author(s) 2023

Methods

MPI-ESM and JSBACH

The simulations for this study were performed using either the MPI-ESM1.2 (ref. 44) in coupled mode or its land surface component JSBACH3 in standalone mode. In particular, the parametrizations of the high-latitude carbon cycle in JSBACH involve large uncertainties, making it difficult to draw robust conclusions from the comparison of single simulations. At the same time, the computational demand of the fully coupled ESM is about 20 times that of the LSM. Thus, to obtain a number of realizations of the biophysical dynamics under a given (hydro)climate trajectory with a reasonable use of resources, we followed a two-step approach that combines coupled MPI-ESM and JSBACH standalone simulations.

In the first step, we performed two coupled simulations which cover the historical period and twenty-first-century warming according to SSP5-8.5. These simulations use different parametrizations of the soil hydrology in the northern permafrost regions, capturing the effects that the ensuing land–atmosphere feedbacks have on the near-surface climate. The coupled simulations are not used to analyse the high-latitude CH₄ emissions directly but, in the second step, we used the atmospheric conditions of each of the simulations to force a set of standalone simulations. In these JSBACH-only simulations, we varied key biophysical parametrizations and initial conditions to account for some of the main uncertainties in the projected greenhouse gas emissions from permafrost-affected soils. With respect to the physics, these standalone simulations are largely consistent with the coupled simulation that provided the forcing, even though there are some deviations whenever the variations in the biophysical assumptions have a strong effect on the simulated vegetation dynamics. However, compared with the impacts that the diverging soil hydrological parametrizations have on the near-surface climate, these constitute second-order effects.

The standard version of JSBACH includes a number of parametrizations that are not well suited for the specific conditions that are characteristic of the Arctic and sub-Arctic region. Most importantly, it does not account for the freezing of water at subzero temperatures and, consequently, neglects the effects of soil ice on percolation and drainage. Thus, the coupled simulations use an adapted JSBACH version that is based on the soil physics developed by refs. 60,61 and includes the phase change of water within the soil, the effect of water on the soil thermal properties, an organic topsoil layer and a five-layer snow scheme. With respect to the soil hydrology, there are important differences between the implementation by refs. 60,61 and the present model version. Most importantly, the present investigation required a set-up that is more flexible with respect to the representation of infiltration, evapotranspiration, percolation and drainage, allowing the simulation of varying degrees of ‘wetness’ of the northern permafrost regions. Furthermore, neither the standard version nor the model version by refs. 60,61 represents the effects of wetlands on the land–atmosphere interactions. As these constitute an important element of the high-latitude hydrological cycle, we implemented a scheme that accounts for ponding water at the surface and represents the possible formation, expansion and drainage of surface water bodies: the wetland-extent dynamics scheme (WEED). The details of these modifications are described in ref. 43, including a comparison with observations, and in the following we merely give a brief overview of the assumptions that lead to the different hydrological conditions in permafrost-affected areas (see below).

The above modifications improve the representation of the physical processes in permafrost regions, but the standard model also has shortcomings with respect to the high-latitude carbon cycle. These shortcomings do not affect the simulated climate (when the model is run with prescribed atmospheric greenhouse gas concentrations) but result in implausible greenhouse gas emissions from permafrost-affected soils. Consequently, the standalone simulations use a different model version in which the representation of soil organic

matter has been adapted to better capture the specific conditions and processes in the Arctic and sub-Arctic region. In JSBACH, the soil carbon dynamics are simulated by the Yasso model, which determines the decomposition rates based on the surface temperature and precipitation rates^{62,63}. This approach is problematic for permafrost-affected regions, where large amounts of soil organic matter are located at depths of several metres. The conditions at these depths are (partly) decoupled from the daily and seasonal cycles at the surface, and the respective decomposition rates cannot be approximated using the moisture fluxes and temperatures at the land–atmosphere interface. For the model version used in this study, we implemented a vertical discretization of the belowground carbon pools, allowing us to determine the decomposition rates using the depth-dependent soil temperature and liquid soil water content. Furthermore, the standard JSBACH model does not distinguish between decomposition under oxic and anoxic conditions, and the CH₄ release from water-saturated soils is not taken into consideration. Here we implemented the CH₄ module proposed by ref. 59, which determines CO₂ and CH₄ production in the soil; the transport of CO₂, CH₄ and O₂ through the three pathways of diffusion, ebullition and plant aerenchyma; and the oxidation of CH₄ in oxygen-rich layers of the soil.

Besides the wetland area determined by the WEED scheme, the CH₄ model uses a TOPMODEL-based approach to estimate an additional grid-cell fraction with saturated soils⁶⁴. The implementation of this second wetland component was required because the WEED scheme merely captures the wetland formation due to depression storage, while in reality many wetlands—in particular, peatlands—are sustained by low drainage rates. The approach makes use of the compound topographic index whose distribution determines a waterlogged grid-cell fraction depending on the mean water table depth. Here the likelihood of waterlogging of a given area within a grid cell is determined by the size of the respective catchment area and the local slope. A key assumption of the approach is that a change in the mean water table does not induce a similar shift in the wetland water table but narrows or widens the wetland water table distribution. In the case of a drop in the mean water table, the CH₄-producing areas that previously had a low water table turn into non-wetlands, a fraction of the previously waterlogged areas now have a lower water table and some areas retain a high water table. Thus, while the overall wetland area is shrinking or expanding, the ratio of wetlands with a high versus a low water table is not drastically altered and the average wetland water table remains comparatively stable. It should be noted that the compound topographic index, as used in our implementation of the TOPMODEL approach, does not take the soil properties into account, which may be problematic with respect to peatlands, where the drainage resistance may not depend on the slope but rather on the low hydraulic conductivity of humified peat. Despite this shortcoming, the simulated wetland area in the northern high latitudes slightly exceeds observation-based values (probably because the observation-based values do not account for wetlands without standing water at the surface and those under forest canopy)⁵⁹. Furthermore, it should be noted that the wetlands determined by the assumed subgrid-scale distribution of the water table have no effect on the physical processes in the model and merely provide an additional grid-cell fraction in which the decomposition of soil organic matter produces CH₄. A detailed description of this model version is given in ref. 13, and Supplementary Methods contain a detailed description of how the model is being used in the context of this investigation.

Observation-based CH₄-emission–temperature dependencies

Besides performing the above-described set of simulations based on variations in the biophysical parameterizations of the model, we followed an additional approach to counter some of the uncertainties in the projected CH₄ fluxes. Here we deduced observation-based temperature–CH₄-emission relationships and used them to estimate wetland CH₄ emissions for the near-surface temperatures simulated for the wet

and the dry scenarios, respectively. Rather than explicitly representing a specific process or a sequence of soil processes leading to CH₄ emissions (for example, CH₄ production, transport and oxidation), these temperature-dependence formulations aim at capturing the net effect of (soil) temperature on CH₄ emissions while also taking into account potential temperature dependencies of plant communities or even wetland types. This high level of abstraction required a broad database encompassing a range of climate and soil conditions across different ecosystem and wetland types. Furthermore, the temperature-driven CH₄ flux model needed to allow for flux projections under future Arctic conditions, which means that present-day observations of Arctic wetland CH₄ fluxes do not provide a sufficient data basis to derive the required temperature–CH₄-emission relationships. Here we used a space-for-time substitution, assuming that future conditions in Arctic wetlands can be approximated by present-day wetland conditions in warmer regions. In our experiments, the terrestrial Arctic warms by around 7 °C to 9 °C during the twenty-first century. Thus, with a latitudinal temperature gradient of roughly 0.7 °C per degree latitude⁶⁵, the future conditions in the region north of 60° N could resemble the present-day conditions in regions as far to the south as 45° N.

To have sufficient data to make a robust space-for-time substitution and account for the potential temperature dependencies of wetland type and ecosystem composition, we combined the site measurements of three datasets. We used the FLUXNET-CH₄ global, multi-ecosystem dataset⁵⁶ (FLUXNET), comprising half-hourly CH₄ fluxes and meteorological variables from 78 sites. Besides limiting the analyses to sites north of 45° N, we selected data only from sites classified as natural wetland ecosystems (bogs, fens and wet tundra), while sites classified as agricultural and upland were omitted, leaving 24 sites to be used in the analyses. Furthermore, we included the data compiled by Yvon-Durocher et al.⁵⁸ (YVON) into the analysis, which is a database of CH₄ emissions and temperatures measured seasonally for 127 field sites that span the globe and encompass wetlands, rice paddies and aquatic ecosystems. Again, we used only those sites located north of 45° N, excluding rice paddies and aquatic systems. As the measurements at most sites were obtained using the eddy covariance technique, we additionally excluded those time series in which the CH₄ fluxes stem from modelled diffusion and chamber measurements, leaving us with six additional sites. Finally, we used the dataset compiled by Chen et al.⁵⁷ (CHEN) comprising seasonal CH₄ emissions from a wide range of wetland ecosystem types and hydrological regimes. From the 204 field sites encompassed in the dataset, we used only those that are located north of 45° N, excluding drained sites, rice paddies and sites where chamber flux measurements were conducted, leaving data from 40 sites for analysis. In total, we analysed the data from 70 sites, 30 of which provided eddy covariance time series and 40 provided chamber time series.

Following ref. 66, we determined the temperature dependence of CH₄ emissions using a nonlinear least squares approach to fit the below function to the measurements:

$$F_{\text{CH}_4} = ab^{((T-T_{\text{ref}})/10)}, \quad (1)$$

where F_{CH_4} is the measured CH₄ flux (mg m⁻² d⁻¹), T_{ref} is the reference temperature (°C), which was taken as the average temperature of a given data sample, T is the temperature (°C) corresponding to the measured CH₄ flux, and a and b are the parameters determined by the fitting process. It should be noted that our approach deviates from the original formulation by ref. 66 in that we omit effects of near-surface turbulence characteristics on CH₄ transport.

In a first step, we derived the temperature dependencies for each of the three datasets individually by fitting the above function to all temperature and CH₄ flux observations contained in a given dataset. However, a representative fit for the combination of all observations across the three datasets was not obtainable in this manner due to the

stark difference in the number of flux records associated with the different observational datasets. At the FLUXNET sites, eddy covariance CH₄ fluxes were estimated quasi-continuously (typically at half-hourly intervals), with the 24 sites providing almost half a million flux records. In contrast, the 40 sites from CHEN are merely represented by 1,484 data points, while the 6 sites from YVON provide 519 data points. Thus, the resulting temperature dependence would have been determined almost exclusively by the data from the 24 FLUXNET sites. To overcome this issue and not bias our estimate of the CH₄ flux temperature dependence as a result of combining the datasets, we limited the information from each site to a maximum of ten flux–temperature pairs. As a first step, we sampled ten temperature values, namely the 5th, 15th, 25th, 35th, 45th, 55th, 65th, 75th, 85th and 95th percentiles of the dataset-specific distribution of temperature observations. Due to the measured CH₄ fluxes associated with these temperature bins showing large variability, we did not use the measured fluxes directly. Instead, we used the temperature models derived for the three individual flux datasets in step 1 to calculate synthetic CH₄ emissions corresponding to the ten temperature percentiles for each of the sites of a given dataset. For sites that contributed less than ten data points, all data were considered. This sampling approach preserves the characteristic CH₄-temperature dependence of each dataset and its general temperature distribution, while not introducing a bias in favour of sites with long, high-frequency time series. The final temperature dependence for a combination of the flux datasets was thus fitted based on 629 data points, with 240 synthetic data points from 24 FLUXNET sites, 299 data points from 40 sites from CHEN, and 54 data points from 6 sites included in YVON—with an almost equal number of data points for eddy covariance and for chamber measurements.

Estimating future CH₄ emissions on the pan-Arctic scale using the above temperature dependence further required a representative annual temperature cycle with a subdaily resolution for the dry and the wet scenarios. For each day of the year, we averaged the simulated minimum and maximum temperatures resulting from a climate stabilization under end-of-the-century greenhouse gas concentrations across the continental Arctic and over a period of 30 years. A synthetic daily cycle was then introduced by connecting the daily temperature minima and maxima using a cosine function. Most of the temperature measurements (at least those for which information on the measurement depths was available) stem from the uppermost 20 cm of the soil, with an average measurement depth of about 10 cm. Thus, to match the depth that best corresponds to the observational basis of the derived temperature–CH₄-emission relationships, we used the temperatures simulated for a depth of 10 cm, for which we interpolated the temperatures of the first (mid-layer depth of 3.25 cm) and the second (mid-layer depth of 15.00 cm) model level using an inverse distance weighting.

MeEP model

Finally, JSBACH accounts for the effects of inundated areas on the surface albedo, vegetation cover, hydrological state of the soil and the land–atmosphere interactions by including a water reservoir on top of the land surface. However, the model does not account for the heat potentially stored in these reservoirs and, in snow-free conditions, the surface energy balance is closed at the top of the soil column. More importantly, JSBACH does not explicitly represent the thermodynamics and biochemistry of water bodies, and the simulated CH₄ emissions represent those of fully saturated soils rather than those of (shallow) lakes and ponds. To be able to provide an estimate for pond emissions for the climate conditions simulated for the wet and the dry scenarios, we used the recently developed MeEP model⁴⁹. MeEP simulates pond CH₄ emissions through the three dominant pathways of CH₄ from ponds (diffusion, ebullition and plant-mediated transport). MeEP consists of a module for the pond physics based on the FLake model⁶⁷, and a soil-heat module for the heat exchange between pond and tundra. The soil-heat module is a simplified version of the permafrost model

CryoGrid^{68–70}. In addition, MeEP features a basic hydrological module to estimate water table fluctuations and a module for the CH₄ dynamics during the ice-covered and open-water season.

For this study, the model was set up for three sites: Lena River Delta (Siberia, Russia), Bylot Island (Nunavut, Canada) and Barrow Peninsula (Alaska, USA). These three sites all feature polygonal tundra, the landscape type for which MeEP was developed. We set the model up using the water-body distribution provided in the PerL database⁷¹. The model was forced with the JSBACH output from the wet and dry simulations (corresponding to a climate stabilization under end-of-the-twenty-first-century greenhouse gas concentrations) linearly interpolated to hourly time steps. The model provides hourly pond CH₄ fluxes from the open water and from the overgrown parts of the ponds. We computed the average annual cycle from the 50 years of model output for each of the three sites in a daily resolution. We then determined the maximum, minimum and average pond CH₄ flux from the three sites separately for the overgrown and open-water pond fraction.

Data availability

The primary data are subject to the terms of the Creative Commons Attribution 4.0 International (CC BY 4.0) licence and available via the German Climate Computing Center long-term archive for documentation data (https://www.wdc-climate.de/ui/entry?acronym=DKRZ_LTA_1219_ds00001).

Code availability

The model and scripts used in the analysis and other Supplementary Information that may be useful in reproducing the authors' work are archived by the MPI for Meteorology and can be obtained by contacting publications@mpimet.mpg.de. The code is subject to the licence terms of the MPI-ESM licence v.2 and will be made available to individuals and institutions for the purpose of research.

References

60. Ekici, A. et al. Simulating high-latitude permafrost regions by the JSBACH terrestrial ecosystem model. *Geosci. Model Dev.* **7**, 631–647 (2014).
61. Ekici, A. et al. Site-level model intercomparison of high latitude and high altitude soil thermal dynamics in tundra and barren landscapes. *Cryosphere* **9**, 1343–1361 (2015).
62. Liski, J., Palosuo, T., Peltoniemi, M. & Sievänen, R. Carbon and decomposition model Yasso for forest soils. *Ecol. Model.* **189**, 168–182 (2005).
63. Tuomi, M., Rasinmäki, J., Repo, A., Vanhala, P. & Liski, J. Soil carbon model Yasso07 graphical user interface. *Environ. Model. Softw.* **26**, 1358–1362 (2011).
64. Beven, K. J. & Kirkby, M. J. A physically based, variable contributing area model of basin hydrology. *Hydrol. Sci. J.* **24**, 43–69 (1979).
65. Zhang, L., Hay, W. W., Wang, C. & Gu, X. The evolution of latitudinal temperature gradients from the latest Cretaceous through the present. *Earth Sci. Rev.* **189**, 147–158 (2019).
66. Wille, C., Kutzbach, L., Sachs, T., Wagner, D. & Pfeiffer, E.-M. Methane emission from Siberian Arctic polygonal tundra: eddy covariance measurements and modeling. *Glob. Change Biol.* **14**, 1395–1408 (2008).

67. Mironov, D. V. *Parameterization of Lakes in Numerical Weather Prediction. Part 1: Description of a Lake Model* Technical Note (German Weather Service, 2006).
68. Langer, M. et al. Rapid degradation of permafrost underneath waterbodies in tundra landscapes—toward a representation of thermokarst in land surface models. *J. Geophys. Res. Earth Surf.* **121**, 2446–2470 (2016).
69. Nitzbon, J. et al. Pathways of ice-wedge degradation in polygonal tundra under different hydrological conditions. *Cryosphere* **13**, 1089–1123 (2019).
70. Juhls, B. et al. Serpentine (floating) ice channels and their interaction with riverbed permafrost in the Lena River Delta, Russia. *Front. Earth Sci.* **9**, 689941 (2021).
71. Muster, S. et al. PerL: a circum-Arctic Permafrost Region Pond and Lake database. *Earth Syst. Sci. Data* **9**, 317–348 (2017).

Acknowledgements

This work was funded by the German Ministry of Education and Research as part of the KoPf-Synthese project (BMBF grant number O3F0834C; P.d.V. and L.K.) and as part of the Palmod project (BMBF grant number O1LP1921A; T.K.), by the German Research Foundation as part of the CLICCS Clusters of Excellence (DFG EXC 2037; P.d.V., L.d.A.G., L.K. and Z.R.), by the European Research Council under the European Union's 691 Horizon 2020 Research and Innovation programme as part of the Q-Arctic project (grant agreement number 951288; P.d.V. and V.B.), and by the European Union's Horizon 2020 Research and Innovation programme as part of the ESM2025 project (grant number 101003536; V.B.).

Author contributions

P.d.V., L.B., L.d.A.G., D.H., T.K., L.K., Z.R. and V.B. designed the experiment. P.d.V., T.K. and Z.R. performed simulations. P.d.V., T.K., Z.R. and V.B. conducted the analysis and validation of simulations. L.B., L.d.A.G., D.H. and L.K. analysed observational data and estimated observation-based temperature–CH₄ flux relationships. All authors contributed to and reviewed the paper.

Funding

Open access funding provided by Max Planck Society.

Competing interests

The authors declare no competing interests.

Additional information

Supplementary information The online version contains supplementary material available at <https://doi.org/10.1038/s41558-023-01715-3>.

Correspondence and requests for materials should be addressed to Philipp de Vrese.

Peer review information *Nature Climate Change* thanks the anonymous reviewers for their contribution to the peer review of this work.

Reprints and permissions information is available at www.nature.com/reprints.